Synthesis, structural characterization and transformation of an eight-electron superatomic alloy, [Au@Ag-19S2P(OPr)(2)(12)]

Yan-Ru Lin, Pilli V. V. N. Kishore, Jian-Hong Liao, Samia Kahlal, Yu-Chiao Liu, Ming-Hsi Chiang, Jean-Yves Saillard, C. W. Liu

Synthesis, Structural Characterization and Transformation of an Eight-Electron Superatomic Alloy, $[Au@Ag_{19}\{S_2P(OPr)_2\}_{12}]$

Yan-Ru Lin,[a] Pilli V. V. N. Kishore,[a, d] Jian-Hong Liao,[a] Samia Kahlal,[b] Yu-Chiao Liu,[c] Ming-Hsi Chiang,[c] Jean-Yves Saillard,*[b] and C. W. Liu*[a]

Controlling the metal nanoclusters with atomic precision is highly difficult and further studies on their transformation reactions are even more challenging. Herein we report the controlled formation of silver alloy nanocluster $[AuAg_{19}\{S_2P(O^nPr)_2\}_{12}]$ (**1**) from an Ag_{20} template via a galvanic exchange route. X-ray structural analysis reveals that the alloy structure comprises of a gold-centered Ag_{12} icosahedron, $Au@Ag_{12}$, capped by seven silver atoms. Interestingly upon reacting with one equiv. of silver(I) salt, (**1**) can transform into a higher nuclearity nanocluster, $[Au@Ag_{20}\{S_2P(O^nPr)_2\}_{12}]^+$ (**2**). The conversion process is studied via ESI mass spectrometry and ^{31}P NMR spectroscopy. This kind of size-structural transformation at the single atom level is quite remarkable. Further the compositions of all the doped nanoclusters (**1**, **2**) were fully characterized with ESI-MS and EDS. The blue shift depicted in the UV-visible and emission spectra for the doped nanoclusters (**1, 2**) comparing with the precursor, Ag_{20}, demonstrates that the doping atoms have significant effects on the electronic structures.

Introduction

During the last decade an increasing interest of research topics was focused on atomically precise nanoclusters (NCs) and alloys. The precise atomic structure is fundamentally important in exploring structure-property relationships. In fact atomically precise, noble metal NCs act as a bridge between metal atoms and nanoparticles.[1] Over the past two decades Au nanoclusters have been actively pursued owing to their unusual stabilities.[2] Very recently the research has been extended to silver following the breakthrough discovery of Ag_{44} by Bigioni and Zheng.[3] A series of Ag nanoclusters Ag_{14},[4] Ag_{16},[5] Ag_{20},[6] Ag_{21},[7] Ag_{25},[8] Ag_{29},[9] Ag_{32},[5] Ag_{34},[10] Ag_{50}[11], Ag_{136}[12] and Ag_{374},[12] have been synthesized and structurally characterized. In the subsequent years, researches on the alloy nanoclusters have gained momentum since alloys have witnessed unique advantages over the homometallic counterparts ranging from enhanced stability, catalytic activity, reactivity and optical properties.[13] In general the alloy clusters are synthesized by either one-pot co-reduction reactions with mixed metal precursors or post-synthetic reactions of a NC with the specific metal precursor.[14] Recently Pradeep and coworkers reported an inter-cluster reaction method for obtaining alloy nanoclusters.[15] To date, a number of atom-precise Au based alloy nanoclusters have been reported. Especially doping on $Au_{25}(SR)_{18}$ was extensively studied with metals such as Cu,[14] Pd,[16] Pt,[16] Ag,[14,17] Cd,[18] and Hg[19]. In contrast, silver-rich alloy nanoclusters are comparatively scarce. Like Au, Ag can also mix with foreign metals such as Pd, Pt, Ni, and Cu at the nanoscale to produce alloy clusters (Ag_4M_2,[20] M = Ni, Pt; Ag_5Pd_4;[21] MAg_{24}, M = Pt, Pd;[22] and $Ag_{28}Cu_{12}$[23]) with different compositions. In the past few years, reports of Ag-Au nanoalloys were constantly expanding and their structure–property relationships have been well studied. Prominent examples include $Au_{25-x}Agx$,[24] $Au_{38-x}Agx$,[25] $Au_{24}Ag_{20}$,[26] $Au_{24}Ag_{46}$,[27] Au_x-Ag_{50-x},[11] $Au_{12}Ag_{32}$,[3b] $Au_{25}Ag_2$,[28] $Ag_{28}Au$[29] $Au_{12}Ag_{13}$[30], $Au_{80}Ag_{30}$,[31] $AuAg_{24}$,[32] and Au_4Ag_{13}.[33] Quite recently our group reported the first $Au@Ag_{20}$ alloy nanocluster passivated by selenium ligands.[34]

On the other hand the accessibility of nanoclusters with precise formula and structure makes it possible to investigate their transformations akin to organic ensembles in organic chemistry. However the structural transformations in nanochemistry are very least understood upon comparing to well-documented organic chemistry. Even though the history of nano-chemistry was still very young (two decades), some remarkable transformations of Au nanoclusters include Au_{25} to Au_{28},[35] Au_{38} to Au_{36},[36] and Au_{144} to Au_{133},[37] were known. Bakr *et al*. has studied these transformations in silver nanoclusters by employing ligand exchange methods.[38] Recently Zhu and coworkers reported a bimetallic Pt_1Ag_{28} nanocluster that was obtained by etching Pt_1Ag_{24} with thiol ligands.[39] Further transformation of $Au_{23-x}Agx$ to Au_{24}-xAgx has also been reported.[40]

$[Ag_{20}\{S_2P(O^nPr)_2\}_{12}] \xrightarrow[THF]{Au(PPh_3)Cl} [Au@Ag_{19}\{S_2P(O^nPr)_2\}_{12}] + AgCl \quad (1) \xrightarrow[THF]{Ag^+} [AuAg_{20}\{S_2P(O^nPr)_2\}_{12}]^+ \quad (2)$

Scheme 1

Lately we developed a new approach in using dithiolate-type ligands in the preparation of two 8-electron superatomic silver NCs, $[Ag_{21}\{S_2P(OR)_2\}_{12}]^+$, and $[Ag_{20}\{S_2P(OR)_2\}_{12}]$.[7,8] We also demonstrated the possibility of controlled reversible transformations of the Ag_{20} to Ag_{21} NCs by adding either Ag^I or $[BH_4]^-$ to the precursors. Inspired by the aforementioned successful findings on silver alloy clusters and their structural transformations, we considered it will be of great interest to employ either Ag_{20} or Ag_{21} NCs as potential templates in producing doped NCs by using galvanic exchange methods and further study the NCs reactivity towards transformations. Herein, we report a new alloy Au-Ag nanocluster formulated as $[AuAg_{20}\{S_2P(O^nPr)_2\}_{12}]^+$ (**2**) which is fabricated from $[AuAg_{19}\{S_2P(O^nPr)_2\}_{12}]$ (**1**) by reacting it with one equiv. of Ag^I salt. For the synthesis of the doped NC $Au@Ag_{19}$ (**1**), a templated galvanic synthesis was adopted.

In a typical synthesis, $[Ag_{20}\{S_2P(O^nPr)_2\}_{12}]$ was firstly dissolved in tetrahydrofuran (THF), then $Au(PPh_3)Cl$ was added instantaneously. The reaction was stirred at −20°C for 2h. The solvents were removed under reduced pressure to obtain a dark red solid. The residue was thoroughly washed with a DCM/water mixture. The DCM layer was separated and dried under vacuum to yield $[AuAg_{19}\{S_2P(O^nPr)_2\}_{12}]$ (**1**). $[AuAg_{20}\{S_2P(O^nPr)_2\}_{12}]^+$ (**2**) was synthesized from (**1**) under similar conditions, except that $Au(PPh_3)Cl$ was replaced by $[Ag(CH_3CN)_4]PF_6$ (Scheme 1).

Results and Discussion

To confirm the nanocluster formula of **1** and to probe the charge state of the cluster, we performed an electrospray ionization mass spectrometric analysis (ESI-MS). Firstly in the mass spectrum no residual peak corresponding to $[Ag_{20}\{S_2P(O^nPr)_2\}_{12}]$ (m/z 4716.30) was observed indicating that the precursor was totally consumed. However we could not observe the expected species, $Au@Ag_{19}$, a peak at m/z 4805.37. Instead, in the positive ESI-MS spectrum of **1** a set of adduct peaks at m/z 4913.23 (calcd 4913.27) and 5001.33 (calcd 5001.34) corresponding to the molecular formulae $[AuAg_{20}\{S_2P(O^nPr)_2\}_{12}]^+$ and $[Au_2Ag_{19}\{S_2P(O^nPr)_2\}_{12}]^+$, respectively, were identified (Figure 1). Furthermore, an additional peak (m/z 2177.19) in **1** at the lower mass region attributed to $[Ag_8Cl\{S_2P(O^nPr)_2\}_6]^+$ has also been observed. The molecular formula assignments for the unexpected products were further confirmed by their experimental isotopic distribution patterns that match closely with the simulated patterns. Actually, the ESI-MS data clearly indicate that there has been a clear replacement of Ag by Au in the $[Ag_{20}]$ precursor (Scheme 1). Furthermore, the results also reveal that the total number of metal atoms in the identified $[AuAg_{20}\{S_2P(O^nPr)_2\}_{12}]^+$ and $[Au_2Ag_{19}\{S_2P(O^nPr)_2\}_{12}]^+$ species were not preserved at 20 but increased to 21. We hypothesized that $Au@Ag_{19}$ might have relatively deprived protecting capability for the metal core due to a limited structural stability embarked on its NC surface in such harsh gas phase conditions. Therefore, only the alloy NCs ($AuAg_{20}$ and Au_2Ag_{19}) with good stability could finally survive. This is not very surprising since there are instances where NCs are transformed into other species of different stabilities in gas phase conditions.[6] Nevertheless the structure of $Au@Ag_{19}$ has been confirmed by single crystal X-ray diffraction analysis (vide infra). The ESI-mass results of **1** particularly spurred our interest to investigate the transformation reaction of $Au@Ag_{19}$ to $AuAg_{20}$. So the reaction of $[Au@Ag_{19}\{S_2P(O^nPr)_2\}_{12}]$ with one equiv. of $Ag(CH_3CN)_4PF_6$ in THF was processed. We observed an immediate color change in the reaction. ESI-MS of the purified product gave rise to the same intense peak at m/z ~ 4913.23 attributable to $[Au@Ag_{20}\{S_2P(O^nPr)_2\}_{12}]^+$ (**2**) (Figure 2). The ESI-MS indicates the purity and the atomic monodispersity of the as-synthesized product. Experimental data matched well with the simulation (see inset) for the assigned molecular formula. Furthermore, in the ^{31}P NMR spectrum, $[Au@Ag_{20}\{S_2P(O^nPr)_2\}_{12}]^+$ exhibits a sharp peak at 103.75 ppm (

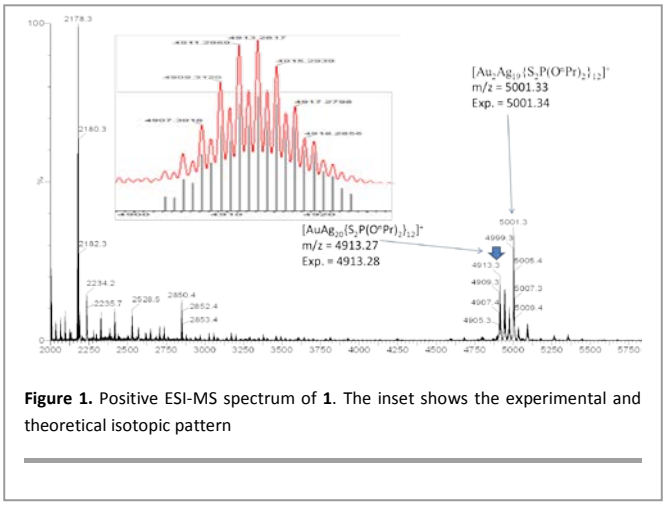

Figure 1. Positive ESI-MS spectrum of **1**. The inset shows the experimental and theoretical isotopic pattern

†ESI figure S1), much different from that in $[Au@Ag_{19}\{S_2P(O^nPr)_2\}_{12}]$ which resonates at comparatively downfield regions (105.6 ppm) (Figure S2 †ESI). We also identified a PF_6 anion in the ^{31}P NMR spectrum that additionally confirms that **2** is a positively charged NC. The

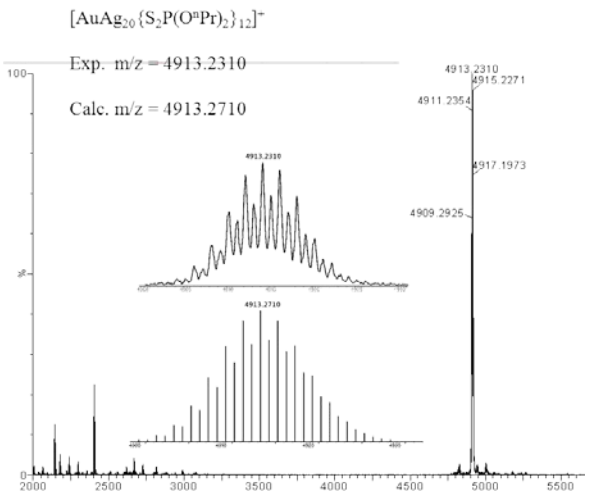

Figure 2. Positive ESI-MS spectrum of **2**. The inset shows the experimental and theoretical isotopic patterns.

single sharp signal in ^{31}P NMR spectra could be possibly due to fast exchange process of chemically nonequivalent dtp ligands, much faster than the NMR time scale. Though the above observations clearly demonstrates the transformation of Au@Ag_{19} to Au@Ag_{20}, we were unfortunately unable to grow single crystals of $[Au@Ag_{20}\{S_2P(O^nPr)_2\}_{12}]^+$ suitable for X-ray diffraction studies. It should be mentioned that a related Au@Ag_{20} cluster has been recently reported by us; namely $[AuAg_{20}\{Se_2P(OEt)_2\}_{12}]^+$, which exhibits an Au@$Ag_{12}$ centered icosahedron surrounded by 12 diselenophosphate (dsep) ligands and 8 Ag capping atoms in a cubic arrangement.[34] So herein for the mechanistic approach, we assume that, under galvanic reduction conditions, Ag_{20} reduces Au^I to Au which at the same time gets into the icosahedral framework to replace the central Ag atom which is likely to be subsequently integrated on the cluster surface as an Ag^I capping atom, leading to the monocationic species of higher nuclearity $[AuAg_{20}\{S_2P(O^nPr)_2\}_{12}]^+$. We assume that the incorporation of the exuded Ag^+ atom onto the NC surface is related to structural stability and shape flexibility factors associated with the NC outer shell, and not to the stable 8-electron superatomic core, since both $[AuAg_{19}\{S_2P(O^nPr)_2\}_{12}]$ and $[AuAg_{20}\{S_2P(O^nPr)_2\}_{12}]^+$ have the same $[Ag_{13}]^{5+}$ core. It is worthy to mention that the $[Au_2Ag_{19}\{S_2P(O^nPr)_2\}_{12}]^+$ NC identified in the ESI-MS of **1** has also an 8-electron count. An important conclusion that we can draw from here is the total atom number in the NC is altered to 21, further confirming that structural stability (with 21 residual atoms) is the fundamental driving factor for the transformations. Since these reactions are instantaneous, it is not possible to identify the intermediates. Nevertheless in order to confirm our mechanistic assumption we synthesized yet another alloys (Au@Ag_{19}) derived from isobutyl and isopropyl groups. The ESI-MS of the synthesized products revealed that Au@Ag_{19} has been transformed into Au@Ag_{20} further confirming structural stability is the solo driving force (Figure S3). Interestingly this kind of cluster transformation phenomenon at a single atom level has not been observed in either Ag or Au doped-NCs. Though there are some reports, most of them come from either ligand exchange methods or etching methods whose mechanisms are not very well understood.[39-40] Indeed our experiments have shown fairly detailed mechanistic aspects of the transformation at the single atom level. However, there is still a lack in our understanding of the reasons for this structural transformation particularly in the interplay of energetic and kinetic factors.

The compositional and structural assumption from mass spectrometry of **1** was further confirmed by single-crystal X-ray analysis. The structural elucidation[41] of **1** reveals a basic framework similar to that of previously reported Ag_{20} NCs. It is composed of a central Au atom surrounded by 12 Ag atoms; these 13 atoms constitute the inner icosahedral core (Figure 3b). The refinement to Au atom is only successful for the central position. However, the 12 icosahedral Ag atoms have 100 % occupancy, confirming that Au selectively occupies the central position. The NC shell of **1** is composed of 12 dtp ligands and 7 capping silver atoms, arranged on 7 of the 20 triangular faces of the Ag_{12} icosahedron (Figure 3b). Two capping silver atoms on any of the two adjacent triangular faces resemble a butterfly motif with the hinge positions defined by their common triangular edges. The Ag-Ag distances in the centered icosahedral core were found in the range of 2.871(12)-2.993(13) Å and are similar to the previously reported Ag_{20} 2.8605(5)–3.0111(5),[6] Ag_{21} 2.842–2.998,[7] Ag_{25} 2.8209–2.9975,[8] and Au@Ag_{24} 2.861–2.978.[32] The

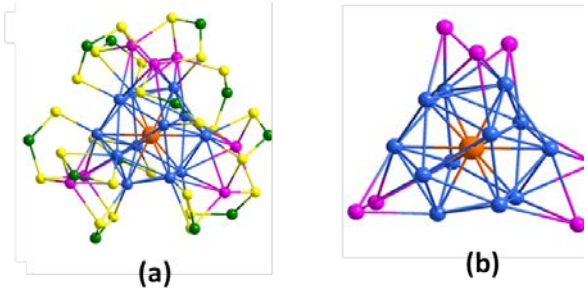

Figure 3: a) X-ray structure of the $[AuAg_{19}\{S_2P(O^nPr)_2\}_{12}]$ cluster with the n-propoxy groups omitted for clarity. b) The Au@Ag_{19} core consisting of a centered icosahedron Au@Ag_{12} and seven capping Ag atoms (crimson). Color code: Au orange, Ag crimson and blue, S yellow, P green.

Ag_{ico}-Ag_{cap} distances 2.9794(13)-3.1230(13) are found to be larger than the Ag_{ico}-Ag_{ico} ones. The Au–Ag icosahedron distances are in the order of 2.6945(8)-2.8136(10), closer to that in Au@Ag_{24}[32] 2.7443–2.7921 and Au@Ag_{20},[34] 2.777(1) Å.

Regarding the connectivity patterns of the dithiolates in **1**, they are the same as those found in the precursor. The average bond lengths of Ag_{ico}-S and Ag_{cap}-S are 2.650 Å and 2.520 Å, respectively, and the S···S bite distance is 3.419(4) Å. All these bond metric values are well matched with the Ag_{20} parent 2.72 Å, 2.51 Å and 3.401(5) Å. The seven Ag_{cap} atoms are held in nearly planar AgS_3 coordination environment with

the dtp ligands whereas it is AgS_2 or AgS with respect to the Ag_{ico} atoms.

The composition of both alloy clusters **1** and **2** were analyzed by using energy-dispersive X-ray spectroscopy (EDS) (Figure S4, S5 ESI†). The EDS results of **1** and **2** (Au/Ag/S/P atomic ratio to be 1.75: 35.21: 42.23: 20.81 for **1** and 1.74: 35.00: 42.32: 20.94 for **2**) are in good agreement with the calculated values of the existing elements (table 2 ESI†). Further the XPS spectra of **(1)** reveals two characteristic peaks at binding energies 84.33 eV and 367.78 eV (Figure S6 ESI†), that corresponds to Au^0 and Ag^I respectively.[42,6] The UV-Vis spectrum of $[Ag_{20}\{S_2P(O^nPr)_2\}_{12}]$ displays two apparent peaks at 359nm and 427nm, respectively (Figure 4 left side). However the spectra of **1** and **2** are significantly different from that of their $[Ag_{20}]$ parent, suggesting there were profound effects of the incorporation of an Au heteroatom. In the doped Ag_{20} nanoclusters it was found that the 427 nm peak was blue-shifted to 420 nm (**1**, **2**) with apparent decrease in intensity. Further we also found that the absorption peak at 359 nm was red-shifted to 386 nm (**1**) and 375nm (**2**) with increased intensity. This trend is different from the earlier reported $Au_{12}Ag_{32}$,[3b] $AuAg_{24}$,[32] and $AuAg_{28}$[29] wherein the clusters display only a blue shift. These results clearly demonstrate that the doping of gold atoms has a different influence towards optical behavior of **1**.

We have also studied the emission properties of **1** and **2**. A comparison of the photoluminescence (PL) spectrum of Ag_{20}, $AuAg_{19}$ (**1**) and $AuAg_{20}$ (**2**) is shown in Figure 4 (right side). The parent cluster Ag_{20} exhibits a characteristic emission band in the near-IR region at about 835 nm at 77K. The PLs of $AuAg_{19}$ and $AuAg_{20}$ show a clear blue shift from 835 nm to 782 nm and 745 nm with an increase in the luminescence intensity up to eight-fold. Interestingly the photoluminescence behavior is very similar to the recently reported $AuAg_{20}$,[34] $AuAg_{24}$,[32] and Ag_xAu_{25-x},[43] but the result deviates from $Au@Ag_{28}$, which shows a red shift after doping.

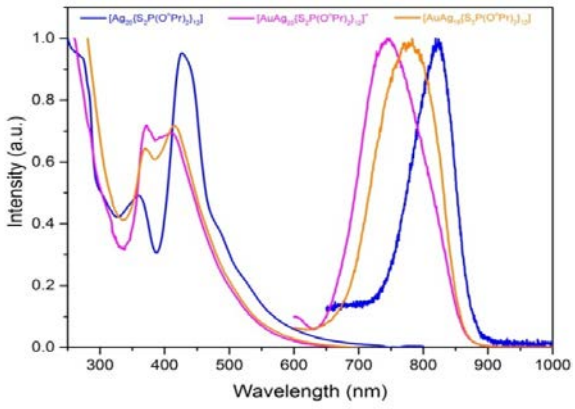

Figure **4**: Normalized UV-Vis absorption (298K), and emission spectra (77K), of $[Ag_{20}\{S_2P(O^nPr)_2\}_{12}]$ (blue line), $[AuAg_{19}\{S_2P(O^nPr)_2\}_{12}]$ (**1**) (orange line) and $[AuAg_{20}\{S_2P(O^nPr)_2\}_{12}]^+$ (red line) (**2**).

DFT calculations[44] have been carried out on simplified models (with dtp = S_2PH_2) of **1**, **2** and their precursor $[Ag_{20}\{S_2P(O^nPr)_2\}_{12}]$, namely **1'**, **2'** and $[Ag_{20}]'$, in order to understand their bonding and stability. Comparing the 20-atom species $[Ag_{20}]'$ and **1**, they have strongly related electronic structures. They are closed-shell superatoms with an 8-electron mixed-valent $[Ag_{13}]^{5+}$ and $[AuAg_{12}]^{5+}$ core, respectively, passivated by 7 outer Ag^+ atoms and 12 dtp^- ligands. In the $[Ag_{20}]'$ cluster the three types of metal atoms have natural atomic orbital (NAO) charges of -044 (center), +0.23 (ico., avg.) and +0.63 (cap., avg.). Thus the more favorable site for a galvanic substitution, *i.e.*, the more electron-rich site, is, by far, the cluster center.[27] This is actually what happens in **1'**, for which the three corresponding NAO metal charges are -0.68 (center), +0.25 (ico, avg.) and +0.62 (cap., avg.). Thus the effect of doping is to increase the polarity within the 13-atom core, so that gold in **1'** can be seen as in the Au(-I) formal oxidation state. The doping increases also the HOMO-LUMO gap which goes from 1.52 eV ($[Ag_{20}]'$) to 1.60 eV (**1**). Since we were not able to grow single-crystals of **2** to determine its structure, we carried out calculations on **2'** assuming the three structures characterized so far for $[Ag_{21}]$ or $[AuAg_{20}]$ NCs, namely of T,[34] C_3[7] or C_1[45] symmetry, respectively. The three structures differ only in the configuration of their passivating shells. TD-DFT calculations[44] carried out on the three structures found the best agreement of the simulated UV-vis spectra with the experimental spectrum of **2** for the C_1 structure (Figure S7 ESI†). We thus assume that **2'** has the C_1 configuration. Its NAO metal charges are -0.65 (center), +0.24 (ico.) and +0.63 (cap., avg.). Clearly, the addition of an Ag^+ ion to **1'** is mainly a local effect on the cluster surface. The TD-DFT simulated spectra of **1'**, **2'** and $[Ag_{20}]'$ (Figure S7 ESI†) are in good agreement with their experimental counterparts. Their low-energy band is associated with a charge density shifting from the central atom to the icosahedron and to the capping Ag atoms. The next absorption bands have more MLCT character.

We have estimated the energy of the transformation of **1** into **2** in the presence of Ag^+ (Scheme 1) by calculating that of the model reaction **1'** + AgCl → **2'** + Cl^- in THF.[44] The process is found exothermic (ΔE = -14 kcal/mol), in agreement with experiment (see above). On the other hand, adding a supplementary Ag^+ ion to **2'** appears unfavorable at the level of modelization.

Conclusions

In summary a new alloy NC $[AuAg_{19}\{S_2P(O^nPr)_2\}_{12}]$ was successfully synthesized by galvanic replacement methods starting from an Ag_{20} template. The structural analysis has been established by single crystal X-ray diffraction studies. We also report the transformation of $[AuAg_{19}\{S_2P(O^nPr)_2\}_{12}]$ into $[AuAg_{20}\{S_2P(O^nPr)_2\}_{12}]^+$ via reactions with Ag^I salts under low temperature. Further insights into the transformation process were obtained by monitoring it with ESI-MS spectrometry and also by ^{31}P NMR spectrum. Presumably shape flexibility of the cluster envelope and structural stability associated with the doped nanocluster $[AuAg_{20}\{S_2P(O^nPr)_2\}_{12}]^+$ are the key factors for this transformation. This work adds a new dimension to the

recently established transformation chemistry of nanoclusters that involves size-structure transformations.

Conflicts of interest

"There are no conflicts to declare".

Acknowledgements

Financial support from the Ministry of Science and Technology in Taiwan (MOST 106-2113-M-259-010) is greatly acknowledged. The GENCI French national computer center is acknowledged for computational resources (grant A0010807367).

Notes and references

1 (a) R. Jin, C. Zeng, M. Zhou, and Y. Chen *Chem. Rev.*, 2016, **116**, 10346–10413. (b) R. R. Arvizo, S. Bhattacharyya, R. A. Kudgus, K. Giri, R. Bhattacharya, P. Mukherjee, *Chem. Soc. Rev*. 2012, **41**, 2943 – 2970. (c) M.-C. Daniel, D. Astruc, *Chem. Rev*. 2004, **104**, 293–346; d) A. C. Templeton, W. P. Wuelfing, R.W. Murray*, Acc. Chem. Res.* 2000, **33**, 27 – 36.

2 (a) H. Qian, M. Zhu, Z.Wu, R. Jin, G. Li, R. Jin, *Acc. Chem. Res.* 2012, **45**, 1470 – 1479. (b) J. F. Parker, C. A. Fields-Zinna, R. W. Murry, *Acc. Chem. Res.* 2010, **43**, 1289 – 1296. (c) P. D. Jadzinsky, G. Calero, C. J. Ackerson, D. A. Bushnell, R. D. Kornberg, *Science* 2007, **318**, 430 – 433. (d) M.W. Heaven, A. Dass, P. S. White, K. M. Holt, R.W. Murray, *J. Am. Chem. Soc.* 2008, **130**, 3754 – 3755. (e) M. Zhu, C. M. Aikens, F. J. Hollander, G. C. Schatz, R. Jin, *J. Am. Chem. Soc.* 2008, **130**, 5883–5885. (f) H. Qian,W. T. Eckenhoff, Y. Zhu, T. Pintauer, R. Jin, *J. Am. Chem. Soc*. 2010, **132**, 8280 – 8281. (g) C. Zeng, H. Qian, T. Li, G. Li, N. L. Rosi, B. Yoon, R. N. Barnett, R. L. Whetten, U. Landman, R. Jin, *Angew. Chem. Int. Ed.* 2012, **51**, 13114 – 13118. (h) C. Zeng, T. Li, A. Das, N. L. Rosi, R. Jin, *J. Am. Chem. Soc*. 2013, **135**, 10011 – 10013. (i) X.-K. Wan, S.-F. Yuan, Z.-W. Lin, Q.-M. Wang, *Angew. Chem. Int. Ed.* 2014, **53**, 2923 – 2926.

3 (a) A. Desireddy, B. C. Conn, J. Guo, B. Yoon, R. N. Barnett, B. N. Monahan, K. Kirschbaum, W. P. Griffith, R. L. Whetten, U. Andmann, T. P. Bigioni, *Nature* 2013, **501**, 399 – 402. (b) H. Yang, Y. Wang, H. Huang, L. Gell, L. Lehtovaara, S. Malola, H. Hakkinen, N. Zheng, *Nature Commun.* 2013, **4**, 2422.

4 H. Yang, J. Lei, B.Wu, Y.Wang, M. Zhou, A. Xia, L. Zhenga, N. Zheng, *Chem. Commun*. 2013, **49**, 300 – 302.

5 H. Yang, Y. Wang, N. Zheng, *Nanoscale* 2013, **5**, 2674 – 2677.

6 R. S. Dhayal, Y.-R. Lin, J.-H. Liao, Y.-J. Chen, Y.-C. Liu, M.-H. Chiang, S. Kahlal, J.-Y. Saillard, C. W. Liu, *Chem. Eur. J.* 2016, **22**, 9943 – 9947.

7 R. S. Dhayal, J.-H. Liao, Y.-C. Liu, M.-H. Chiang, S. Kahlal, J.-Y. Saillard, C. W. Liu, *Angew. Chem. Int. Ed*. 2015, **54**, 3702 – 3706.

8 C. P. Joshi, M. S. Bootharaju, M. J. Alhilaly, O. M. Bakr, *J. Am. Chem. Soc*. 2015, **137**, 11578–1158.

9 L. G. AbdulHalim, M. S. Bootharaju, Q. Tang, S. d. Gobbo, R. G. AbdulHalim, M. Eddaoudi, D.-E. Jiang, O. M. Bakr, *J. Am. Chem. Soc.* 2015, **137**, 11970–11975.

10 D. Sun, G.-G. Luo, N. Zhang, R.-B. Huang, L.-S. Zheng, *Chem. Commun.* 2011, **47**, 1461 – 1463.

11 W. Du, S. Jin, L. Xiong, M. Chen, J. Zhang, X. Zou, Y. Pei , S. Wang, and M. Zhu *J. Am. Chem. Soc.* 2017, **139**, 1618–1624.

12 H. Yan, Y. Wang, X. Chen, X. Zhao, L. Gu, H. Huang, J. Yan, C. Xu, G. Li, J. Wu, A. J. Edwards, B. Dittrich, Z.Tang, D. Wang, L. Lehtovaara, H. Hakkinen N. Zheng, *Nature Commun*. 2016, **7**, 12809.

13 (a)H. Qian, D.-e. Jiang, G. Li, C. Gayathri, A. Das, R. R. Gil and R. Jin, *J. Am. Chem. Soc.,* 2012, **134**, 16159-16162. (b) S. Wang, X. Meng, A. Das, T. Li, Y. Song, T. Cao, X. Zhu, M. Zhu and R. Jin, *Angew. Chem., Int. Ed.,* 2014, **53**, 2376-2380. (c) Y. Negishi, T. Iwai and M. Ide, *Chem. Commun.,* 2010, **46**, 4713-4715. (d) Y. Negishi, W. Kurashige, Y. Niihori, T. Iwasa and K. Nobusada, *Phys. Chem. Chem. Phys.,* 2010, **12**, 6219. (e) Y. Niihori, W. Kurashige, M. Matsuzaki and Y. Negishi, *Nanoscale*, 2013, **5**, 508.

14 S. Wang, Y. Song, S. Jin, X. Liu, J. Zhang, Y. Pei, X. Meng, M. Chen, P. Li and M. Zhu, *J. Am. Chem. Soc.,* 2015, **137**, 4018-4021.

15 K. R. Krishnadas, A. Ghosh, A. Baksi, I. Chakraborty, G. Natarajan, T. Pradeep*, J. Am. Chem. Soc.* 2016, **138**, 140-148.

16 R. Jin and K. Nobusada, *Nano Res.,* 2014, **7**, 285−300.

17 Q. Li, S. Wang, K. Kirschbaum, K. J. Lambright, A. Das and R. Jin, *Chem. Commun.,* 2016, **52**, 5194−5197.

18 C. Yao, Y.-j. Lin, J. Yuan, L. Liao, M. Zhu, L.-h. Weng, J. Yang and Z. Wu, *J. Am. Chem. Soc.*, 2015, **137**, 15350- 15353.

19 L. Liao, S. Zhou, Y. Dai, L. Liu, C. Yao, C. Fu, J. Yang and Z. Wu, *J. Am. Chem. Soc.,* 2015, **137**, 9511-9514

20 (a) S. R. Biltek, S. Mandal, A. Sen, A. C. Reber, A. F. Pedicini, S. N. Khanna, *J. Am. Chem. Soc.* 2012, **135**, 26−29. (b) S. R. Biltek, A. Sen, A. F. Pedicini, A. C. Reber, S. N. Khanna, *J. Phys. Chem*. A 2014, **118**, 8314−8319.

21 S. Sarkar, I. Chakraborty, M. K. Panwar, T. Pradeep, *J. Phys. Chem. Lett.* 2014, **5**, 3757−3762.

22 J. Y. Haifeng, H. Su, H. Yang, S. Malola, S. Lin, H. Häkkinen, N. Zheng, *J. Am. Chem. Soc.* 2015, **137**, 11880–11883.

23 J. Yan, H. Su, H. Yang, C. Hu, S. Malola, S. Lin†, B. K. Teo, H. Häkkinen, and N Zheng *J. Am. Chem. Soc.* 2016, **138**, 12751–12754.

24 Q. Li, S. Wang, K. Kirschbaum, K. J. Lambright, A. Dasa and R. Jin *Chem. Commun.,* 2016, **52**, 5194-5197.

25 C. Kumara, K. J. Gagnon, and A. Dass, J. Phys. Chem. Lett. 2015, **6**, 1223−1228.

26 Y. Wang, H. Su, C. Xu, G. Li, L. Gell, S. Lin, Z. Tang, H. Häkkinen, and N. Zheng, *J. Am. Chem. Soc.* 2015, **137**, 4324−4327.

27 S. Wang, S. Jin, S. Yang, S. Chen, Y. Song, J. Zhang, M. Zhu, *Sci. Adv.* 2015, **1**, e1500441.

28 C. Yao, J. Chen, M. Li, L. Liu, J. Yang, and Z. Wu, *Nano Lett.* 2015, **15**, 1281−1287.

29 G. Soldan, M. A. Aljuhani, M. S. Bootharaju, L. G. AbdulHalim, M. R. Parida, A.-H. Emwas, O.F. Mohammed, O. M. Bakr, *Angew. Chem., Int. Ed.* 2016, **51**, 5749-5753.

30 M. Zhou, J. Zhong, S. Wang, Q. Guo, M. Zhu, Y. Pei, A. Xia, *J. Phys. Chem. C.* 2015, **119**, 18790−18797.

31 J-L. Zeng, Z-J. Guan, Y. Du, Z-A. Nan, Y-M Lin, and Q-M Wang *J. Am. Chem. Soc*. 2016, **138**, 7848−7851.

32 (a) M. S. Bootharaju, C. P. Joshi, M. R. Parida, O. F. Mohammed, O. M. Bakr, *Angew. Chem. Int. Ed.* 2016, **55**, 922–926. (b) M.S. Bootharaju, L. Sinatra and O. M. Bakr *Nanoscale,* 2016, 8, 17333-17339.

33 T. Chen, S. Yang, J. Chai, Y. Song, J. Fan, B. Rao, H. Sheng, H. Yu, M. Zhu, *Sci. Adv.* 2017, **3**, no. 8, e1700956.

34 W-T Chang, P-Y Lee, J-H Liao, K. K. Chakrahari, S. Kahlal, Y-C Liu, M-H Chiang, J-Y Saillard, and C. W. Liu *Angew. Chem. Int. Ed.* 2017, **56**, 10178.

35 C. Zeng, T. Li, A. Das, N. L. Rosi, R. Jin, *J. Am. Chem. Soc.* 2013, **135**, 10011−10013.

36 C. Zeng, H. Qian, T. Li, G. Li, NL. Rosi, B. Yoon, RN. Barnett, RL. Whetten, U. Landman, *Angew. Chem., Int. Ed.* 2012, **51**, 13114.

37 C. Zeng, Y. Chen, K. Kirschbaum, K. Appavoo, M. Y. Sfeir, *Sci. Adv.* 2015, **1**, e1500045.

38 (a) M. S. Bootharaju, V. M. Burlakov, T. M. D. Besong, C. P. Joshi, L. G. AbdulHalim, D. M. Black, R. L. Whetten, A. Goriely, and O. M. Bakr *Chem. Mater.* 2015, **27**, 4289−4297. (b) M. S. Bootharaju, C. P. Joshi, L. G. AbdulHalim, J. A. Mohammad, O. M. Bakr, *Chem. Mater.* 2016, **28**, 3292. (c) L. G. AbdulHalim, N. Kothalawala, L. Sinatra, A. Dass, O. M. Bakr, *J. Am. Chem. Soc*. 2014, **136**, 15865.

39 X. Kang, M. Zhou, S. Wang, S. Jin, G. Sun, M. Zhu, R. Jin, *Chem. Sci.* 2017, **8**, 2581-2587.

40 Q Li, M. G. Taylor, K. Kirschbaum, K. J. Lambright, X. Zhu, G. Mpourmpakis, R. Jin, *J Colloid Interface Sci.* 2017, **505**, 1202.

41 Crystallographic data for **1**: $C_{72}H_{168}AuAg_{19}O_{24}P_{12}S_{24}$, Monoclinic, space group $P2_1/c$, a = 29.6903(7) Å, b = 17.3784(4) Å, c = 30.3868(6) Å, α = 90°, β = 110.3727(9)°, γ = 90°, V = 14697.9(6) $Å^3$, Z = 4, T = 150(2) K, μ = 3.984 mm^{-1}, R_{int} = 0.0273, R1 = 0.0426, wR2 = 0.1012 [I> 2σ(I)]. The goodness of fit on F^2 was 1.033.

42 J. Radnik, C. Mohrb, P. Claus, *Phys. Chem. Chem. Phys.,* 2003, **5**, 172–177.

43 M. Zhou, J. Zhong, S. Wang, Q. Guo, M. Zhu,Y. Pei, and A. Xia *J. Phys. Chem. C* 2015, **119**, 18790−1879.

44 DFT and TDDFT calculations were carried out at the BP86/Def2TZVP and CAM-B3LYP/Def2TZVP levels, respectively (see supplementary informations).

45 Liao, J.-H.; Kahlal, S.; Liu, Y.-C.; Chiang, M.-H.; Saillard, J.-Y.; Liu, C. W. *J. Cluster Sci.* submitted.